Pergamon

PII: S0094-5765(96)00096-3

Acta Astronautica Vol. 38, No. 11, pp. 829–838, 1996

0094-5765/96 $15.00+0.00

ON THE REFRACTION OF SHOCK WAVE OVER A SLOW–FAST GAS INTERFACE

SIMIN ZENG†

Department of Mech. & Aero. Engineering, Rutgers University, PO. Box 909, Piscataway, NJ 08855, U.S.A.

and

KAZUYOSHI TAKAYAMA

Institute of Fluid Science, Tohoku University, Sendai 980, 2-1-1 Katahira, Japan

(Received 15 March 1995; revised version received 24 April 1996)

Abstract—This paper presents a numerical simulation of the shock wave refraction over an interface of two different gases. Harten–Yee upwind TVD scheme is used and an approximate Riemann solver has been developed specially for this problem in which the interface of the two gases can be treated without any peculiar consideration. Some experimental data have been obtained for the refraction of a planar shock at the air/CO_2 and air/He interfaces. The refraction and reflection of the shock wave as well as the flow field around it are visualized by using double exposure holographic interferometry. The numerical simulation results were compared with the experimental results, good agreement was obtained. Based on the one-dimensional piston theory, the conditions for both BPR (Irregular Refraction of the Bound Precursors) into FPR (Free Precursor Refraction) and FNR (Free Precursor von Neumann Irregular Refraction) into TNR (Twin von Neumann Refraction) transitions are analysed. The crater of the gaseous interface near the boundary is also discussed in this work. Copyright © 1996 Elsevier Science Ltd

1. INTRODUCTION

As the wave impedance changes when a planar shock wave crosses to a gaseous interface inhomogeneity, the refraction takes place accompanied by interference of waves at the interface. In recent years, with the studies of the shock-induced mixing for Scram-jet combustors[1] and inertial confinement fusion[2] as well as the extracorporeal shock wave focusing[3,4], the interference of the shock waves with a mixed gas of fuels and the interaction of the shock waves with density inhomogeneities have focused attention as one of the topics of turbulent mixing. This environment has been referred to as the shock-induced Rayleigh–Taylor (RT) instability or the Richtmyer–Meshkov (RM) instability[5,6]. By using the general idea of wave impedance, the regular refraction of the shock wave at a gaseous interface was analytically studied by Polachek and Seeger in 1951[7]. After that, an experimental study concerning this problem was done by Jahn[8]. Mach–Zehnder interferometry was employed in this investigation. The experimental results revealed agreement with the analytical predictions studied by Polachek. By using schlieren photographs, Abd-El-Fattah and Henderson *et al.* visualized the various refraction patterns of the shock wave refraction at the slow–fast (S/F) and fast–slow (F/S) gaseous interfaces and classified them using the shock polar analysis[9–11].

Because the phenomena of the wave refractions at the gaseous interface are very complicated, especially for irregular wave refractions, it is difficult to obtain the analytical solutions, and the idea of wave impedance fails to describe the whole flow field. Therefore, there are still many knotty problems unsolved, such as the conditions for the shock structure transitions on regular and irregular refractions. There is a need for computational simulations and experimental visualizations in order to study these problems in greater detail. Recently, a numerical simulation which agrees with experiments was published[12]. A more complicated case of shock wave refraction on non-planar interfaces was studied by Samtaney and Zabusky[13].

The subject of this paper is the investigation of the shock morphologies in a shocked-oblique S/F gaseous interface. The refraction of the shock wave at air/He, CH_4/H_2, and CO_2/H_2 interfaces are well simulated by using the presented scheme. The results are verified by comparing experimental data of holographic interferometry. Several cases have been calculated by the proposed numerical scheme with various Mach numbers, angles for the incident shock and density ratios for the interface. According to the one-dimensional piston theory and the shock polar analysis, the conditions for the transitions of the shock structures from BPR into FPR and from FNR

†Author for correspondence.

into TNR are investigated. Finally, we will discuss the crater of the gaseous interface near the boundary of the bottom surface of the shock tube as well as the behaviour of the flow in this small region.

2. NUMERICAL SIMULATION

The shock wave refraction at a gaseous interface is normally accompanied by dramatic deformation of the latter. Therefore, to investigate these phenomena numerically, a special algorithm which captures both the shock wave and density interface is needed. Our numerical method is based on the Harten–Yee upwind TVD scheme[14,15], which was extended to the system of shock iterations over the gaseous interface. A special approximate Riemann solver has been developed to capture the gas interface.

The basic equations for a two-dimensional unsteady compressible viscous flow can be written as follows:

$$U_t + F_x + G_y = \frac{1}{\mathrm{Re}}(R_x + S_y). \tag{1}$$

$$U = \begin{bmatrix} \rho_1 \\ \rho_2 \\ \rho u \\ \rho v \\ E \end{bmatrix}, \quad F = \begin{bmatrix} \rho_1 u \\ \rho_2 u \\ \rho u^2 + P \\ \rho uv \\ (E+P)u \end{bmatrix},$$

$$G = \begin{bmatrix} \rho_1 v \\ \rho_2 v \\ \rho uv \\ \rho v^2 + P \\ (E+P)v \end{bmatrix}$$

$$R = \begin{bmatrix} 0 \\ 0 \\ \tau_{xx} \\ \tau_{xy} \\ u\tau_{xx} + v\tau_{xy} + \dfrac{T_x}{\mathrm{Pr}(k-1)} \end{bmatrix}$$

$$S = \begin{bmatrix} 0 \\ 0 \\ \tau_{xy} \\ \tau_{yy} \\ u\tau_{xy} + v\tau_{yy} + \dfrac{T_y}{\mathrm{Pr}(k-1)} \end{bmatrix}, \tag{2}$$

$$\rho = \rho_1 + \rho_2 \tag{3}$$

$$\tau_{xx} = \tfrac{4}{3}u_x - \tfrac{2}{3}v_y \tag{4}$$

$$\tau_{xy} = u_y + v_x \tag{5}$$

$$\tau_{yy} = \tfrac{4}{3}v_y - \tfrac{2}{3}u_x . \tag{6}$$

Here, ρ denotes the density, u and v are the velocity components in x- and y-directions, E is the total energy per unit volume, P is the pressure and T is the temperature, Re and Pr are the Reynolds and Prandtl numbers. Subscripts 1 and 2 indicate air and the second gas, He. For a perfect gas, the pressure is given by

$$P = (k-1)\left[E - \frac{\rho}{2}(u^2 + v^2)\right] \tag{7}$$

and the specific heat ratio

$$k = \frac{\dfrac{k_1\rho_1}{m_1(k_1-1)} + \dfrac{k_2\rho_2}{m_2(k_2-1)}}{\dfrac{\rho_1}{m_1(k_1-1)} + \dfrac{\rho_2}{m_2(k_2-1)}}, \tag{8}$$

where m is the molecular weight.

The solid wall boundary condition was applied on the bottom wall surface. Considering the inlet and outlet sections, the outgoing waves should go through the boundaries by which the flow enters or leaves the computational domain, without producing unphysical reflected waves. The non-reflective boundary condition was situated on the boundaries of the left and right side of the calculation regions as well as the boundary of the upper side of the computational domain.

3. APPARATUS

The experiments were performed in a conventional shock tube which consists of a high pressure section, a low pressure section and a test section; the high pressure section was 1.5 m long and 150 mm i.d., and the low pressure section was 5.6 m long and 60 mm × 150 mm in cross section. The layout of the apparatus is shown in Fig. 1.

In this experiment, the driver gas was high pressure nitrogen (initial pressure, 0.34 MPa), the driven gas was air (initial pressure P_1 is 0.1 MPa, and initial temperature T_1 is 298 K). The average speed of incident shock wave was measured using two pressure transducers (Kistler 603B), placed 250 mm apart, ahead of the test section. A model with gas interface was placed in the test section. The incident shock Mach number was 1.400 ± 0.005.

The test gas conditions are shown in Table 1. Figure 2 shows a test piece to make a gaseous interface, which consists of a base block A and a side block B. The side B is the angle of adjuster while the base A is the leading block. A pair of steel lines were set along the corners of these blocks. The triangle zone made by the lines (see Fig. 2) was wrapped by 0.7 μm thick mylar film (PET film, TORAY Co. Ltd-made) and made airtight by vacuum grease. The gas exchange was made through two holes: one at the base block and another at the side block. Special attention was paid to keep the same pressure across the mylar film, and not to rupture it. In the case of He, air in the triangle zone was absorbed in the

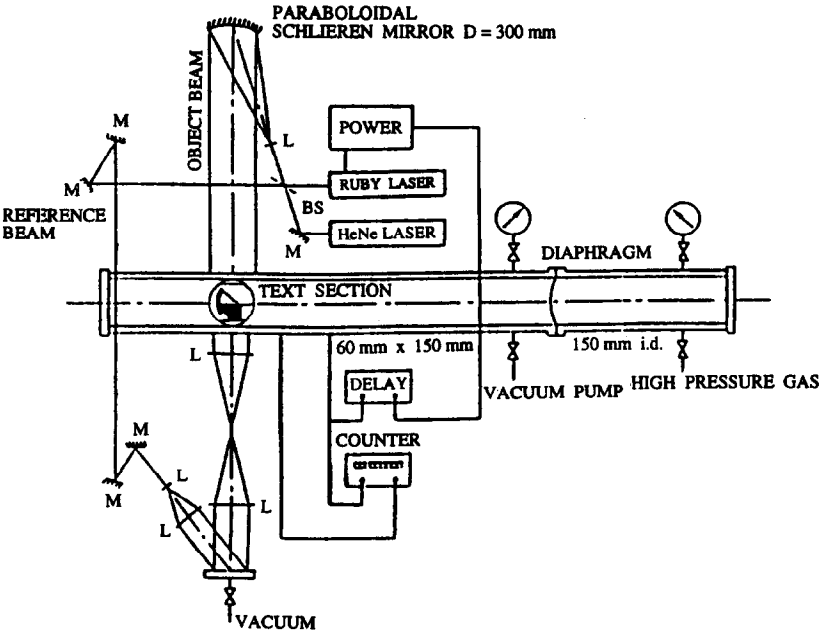

Fig. 1. Schematic diagram of shock tube and optical arrangement.

vacuum through the lower hole. On the contrary, in the case of CO_2, it has been done reversely.

The flow field was visualized by using double exposure holographic interferometry. The optical arrangement is shown in Fig. 1. A double pulse ruby laser (Apollo Laser Inc. 22HD, 694.3 nm wave length, 2 J/pulse and 20 ns pulse duration) was used as a light source. The first exposure was done before the event and the second exposure was synchronized with the event. The interval of the double exposure was 350 μs. In the interferogram, one fringe shift corresponds to density variation $\Delta\rho$ as follows:

$$\Delta\rho = \frac{\lambda}{KL}. \tag{9}$$

Here, K is a Gradstone–Dale constant (0.2247 cm^3/g for air), L is the shock tube width (60 mm) and λ is the wave length of the laser. Thus, one fringe shift corresponds to 4.18% of air density at standard atmosphere in air.

4. THE CONDITION FOR TRANSITION FROM BPR TO FPR

When a planar shock wave collides with an oblique gaseous interface of a Slow/Fast type, it refracts over it either as a Regular Refraction (RR) or as an Irregular Refraction, which depends on the Mach number of the incident shock wave, M_s, and the angle of incident shock, α_i, as well as the characteristic parameters of the gases, such as specific heat ratio, etc.

If α_i is smaller than a critical value, all three shock waves, including the incident shock I, the reflected shock R and the transmitted shock T, are met at a single node X. In this case, two kinds of shock refractions may occur at the gaseous interface. One is called RRR (Regular Refraction with a Reflected Shock) and the other is called BPR (see Fig. 3). As shown in Fig. 3, the typical feature of BPR is that the contours at first diverge as they retract from the reflected shock. They converge into a compression downstream of the refracted shock. According to the von Neumann theory, there is no physically acceptable solution for BPR, and the impedances of the transmitted and reflected waves are

Table 1. Test gas (0.1 MPa, 293 K)

	Molecular weight (g/mol)	Specific heat ratio	Sound speed (m/s)
Air	28.9	1.402	343
He	4.0	1.667	1007
CO_2	44.0	1.301	268
CH_4	16.04	1.307	446

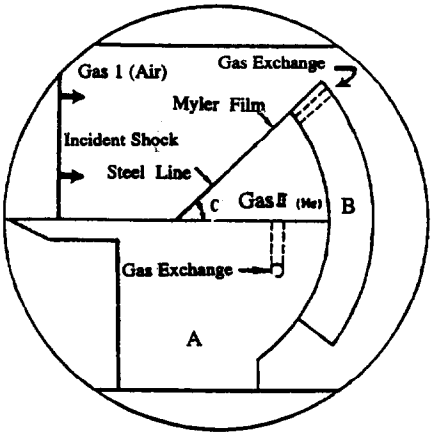

Fig. 2. Schematic diagram of test section.

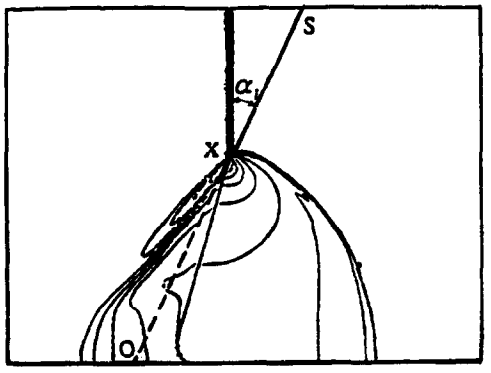

Fig. 3. Irregular refraction of the bound precursor of a planar shock at air/He interface.

unreal. For this reason the system is irregular[12]. Although the shock refraction of BPR type is irregular, the three shock waves, I, R and T, still meet at a single node. Therefore, the configuration of the shock refraction BPR belongs to the same type RRR.

If α_i is increased further, a precursor wave J appears in front of the incident shock, and the three shock waves will not meet at a single node. The respective shock refraction can be called FPR (see Fig. 4). Figure 4 shows that in front of the incident shock there is a free precursor wave J which is caused by the transmitted wave compressed to the gaseous interface from the fast gas. A modified side shock J' is formed when the free precursor disturbs the flow behind the incident shock. Obviously, the reason for the transition of the refraction configuration from BPR to FPR is that the velocity of transmitted shock T propagating in the fast gas is larger than the velocity of the incident shock propagating along the impedance interface.

To discuss the condition for the transition from BPR to FPR, a schematic illustration of the FPR is shown in Fig. 5. By the conservation of mass,

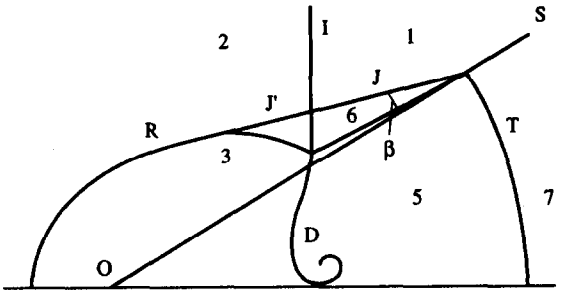

Fig. 5. Schematic illustration of the wave configuration of the free precursor refraction.

momentum and energy for a piston of unit cross-section, we have

$$M_s = \frac{u_s - u_1}{a_1} \tag{10}$$

$$\frac{u_2 - u_1}{a_1} = \frac{2}{k_1 + 1}\left(M_s - \frac{1}{M_s}\right). \tag{11}$$

We assume that the flow velocity in front of the incident shock, u_1, is equal to zero. We can obtain u_2 after a short circulation.

$$u_2 = \frac{2}{k_1 + 1}\left(\frac{V_s^2 - a_1^2}{V_s}\right). \tag{12}$$

In a similar way, we find the velocity of the flow field in state (5)

$$u_5 = \frac{2}{k_2 + 1}\left(\frac{V_t^2 - a_7^2}{V_t}\right), \tag{13}$$

where V and u are the velocities of the shock and the flow, respectively. a is the speed of sound and k is the specific heat ratio. The subscripts for V, u, k and a indicate the states of flow fields which are defined in Figs 5 and 10. The subscripts s and t indicate the incident shock and the transmitted shock.

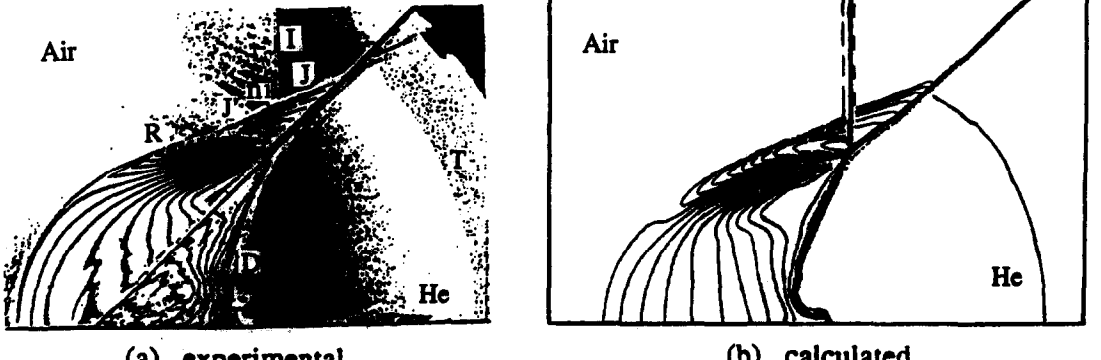

(a) experimental (b) calculated

Fig. 4. Free precursor refraction of a planar shock at air/He interface ($M_s = 1.4$, $\alpha_i = 44°$).

In order to apply (12) and (13) to the free precursor T, we assume that the flow velocity behind the incident shock is equal to the driven gas in the state (5)[10], that is

$$\frac{2}{k_1+1}\left(\frac{V_s^2-a_1^2}{V_s}\right)=\frac{2}{k_2+1}\left(\frac{V_t^2-a_7^2}{V_t}\right) \quad (14)$$

or

$$V_t=\tfrac{1}{2}[b+(b^2+4a_7^2)^{1/2}], \quad (15)$$

where

$$b=\frac{k_2+1}{k_1+1}\frac{V_s^2-a_1^2}{V_s}. \quad (16)$$

The pressure ratio for states (5) and (7) can be obtained from the piston theory

$$\frac{P_5}{P_7}=\frac{2k_2}{k_2-1}M_{st}^2-\frac{k_2-1}{k_2+1}, \quad (17)$$

where

$$M_{st}=\frac{v_t}{a_7}. \quad (18)$$

In order to calculate the Mach number of shock J, M_{st}, and the local wave angles of J and T, β, we apply the piston theory to states (5), (6) and (1)

$$\frac{P_6}{P_1}=\frac{2k_1M_{sj}-(k_1-1)}{k_1+1} \quad (19)$$

$$\frac{P_6}{P_1}=\left[1-\frac{k_2-1}{k_1+1}\frac{a_1}{a_f}\left(M_{sj}-\frac{1}{M_{sj}}\right)\right]^{-2k_2/k_2-1}, \quad (20)$$

then

$$\frac{P_5}{P_1}=\frac{P_5}{P_6}\frac{P_6}{P_1}=\frac{2k_1M_{sj}-(k_1-1)}{k_1+1}\times\left[1-\frac{k_2-1}{k_1+1}\frac{a_1}{a_f}\left(M_{sj}-\frac{1}{M_{sj}}\right)\right]^{-2k_2/k_2-1}, \quad (21)$$

where, M_{sj} denotes the Mach number of precursor shock and a_f is the speed and sound in the fast gas. As the pressures in both states (1) and (7) are the same, and by applying eqn (17), the shock number M_{sj} can be found from eqn (21).

From eqns (18) and (21) the wave angle β can be given by

$$\beta=\sin^{-1}\left(\frac{M_{sj}a_1}{M_{st}a_f}\right). \quad (22)$$

As we mentioned above, the condition for the BPR transitioning to FPR is that the velocity of transmitted shock propagating in the fast gas, V_t, is larger than the velocity of incident shock propagating along the impedance interface, $u_s/\cos\alpha$. According to this condition we assume that I, T and R meet at one node X. α_{cb} is denoted as the critical angle of the incident shock for the transition from BPR to FPR.

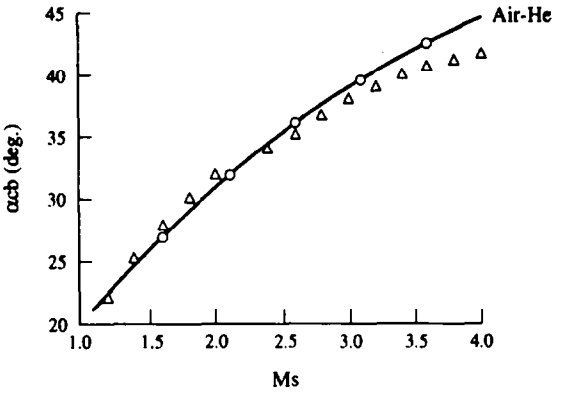

Fig. 6. Comparison of critical angles between the results of the analysis method and the numerical simulation for transition from BPR into FPR.

Thus, an expression for α_{cb} as a function of M_s is given by

$$\alpha_{cb}=\cos^{-1}\left(\frac{a_1}{V_t}M_s\right). \quad (23)$$

Figure 6 is the comparison of the critical angles between both results, calculated by eqn (23) and the method of the numerical simulation. The Slow/Fast gases are air and helium. The calculation results of the critical angles for other Slow/Fast gases are shown in Fig. 7. From the calculation results we can see that the values of the critical angle α_{cb} decreases directly with the strength of the incident shock and that the regular refraction does not only occur at small angles of the incident shock. On the contrary, when the Mach number of the incident shock is large enough, the irregular refraction may occur at small angles of incident shock for some Slow/Fast gas interfaces.

5. THE CONDITION FOR TRANSITION FROM FNR TO TNR

As the angle of the incident shock, α_i, increases, a Mach stem appears on the gaseous interface. This phenomenon is shown in Fig. 8. The Mach stem consists of two parts, n_1 and n_2. n_1 is the wave resulted

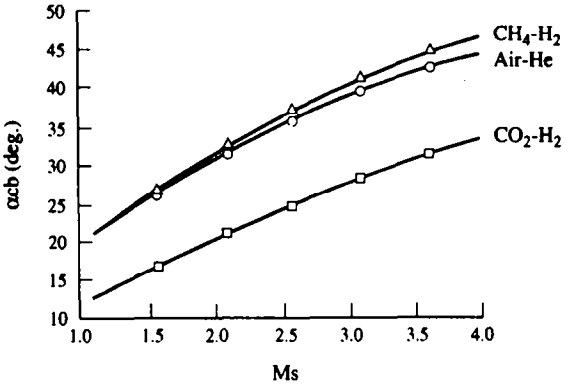

Fig. 7. Critical angles, α_{cb}, as a function of M_s for transition from BPR into FPR.

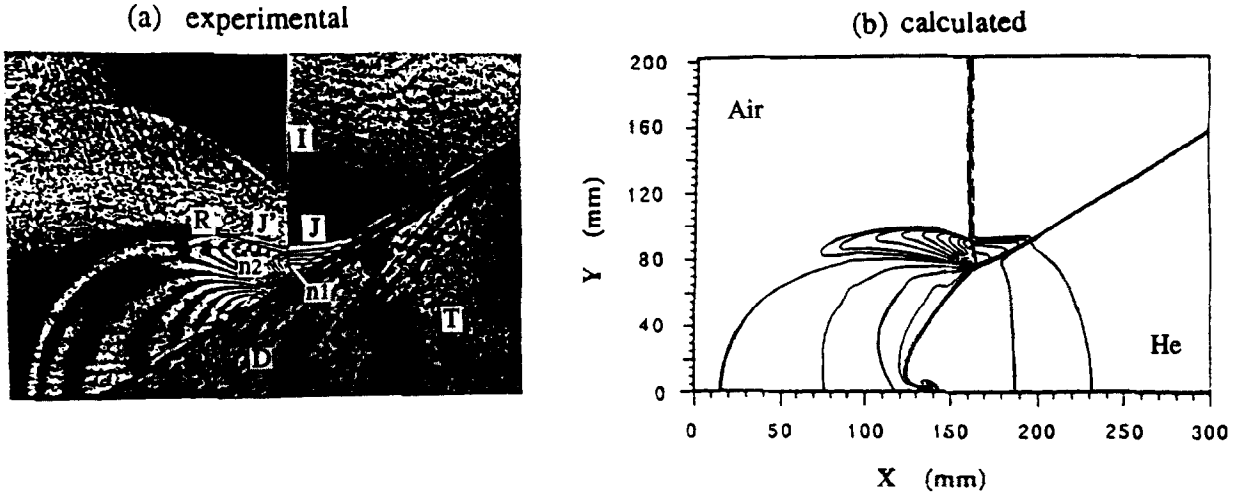

Fig. 8. Free precursor von Neumann irregular refraction of a planar shock at an air/He interface ($M_s = 1.4$, $\alpha_i = 58°$).

from the shock interacting with the incident shock, the reflected shock and the precursor shock. n_2 corresponds to the part of the incident shock wave interacting with the precursor shock. This configuration of the shock refraction is called FNR.

When the angle of incident shock α_i is larger than a certain critical value, the pattern of the shock refraction changes from FNR into another structure. The phenomenon can be seen in Fig. 9. The key feature of the latter shock refraction is the way in which a part of the Mach stem interacts with the precursor wave. This latter part is denoted n_1 while the rest of the Mach stem is referred to as n_3. This pattern of shock refraction is called TNR. Obviously, the strength of the Mach stem for parts n_1 and n_3 differs. As is shown in Fig. 9, the nature of this shock refraction for n_3 is similar to the case of a shock wave reflection on an oblique planar surface. That is, the incident shock interacts only with the reflected wave R. Experiments also show that the part of Mach stem n_3 is almost perpendicular to the gaseous interface. This case can be seen in Fig. 9.

To discuss the condition of FNR into TNR transition, we assume that I, R and J meet at one node X, and the length of n_3 is equal to zero. Therefore, the angle of incident shock α_{cf} corresponding to this case is the condition for FNR into TNR transition. An illustration depicting the case is shown in Fig. 10.

When the Mach reflection occurs on the oblique planar surface, the Mach stem is perpendicular to the wedge surface, as is frequently seen in supersonic flows[16]. Due to both reflection wave and the precursor wave's interaction among the incident shock, the Mach stem n_1 is not perpendicular to the gas interface in the case of irregular shock refraction at a Slow/Fast gaseous interface. n_1 is deflected to the down-stream of the incident shock. Obviously, it is a

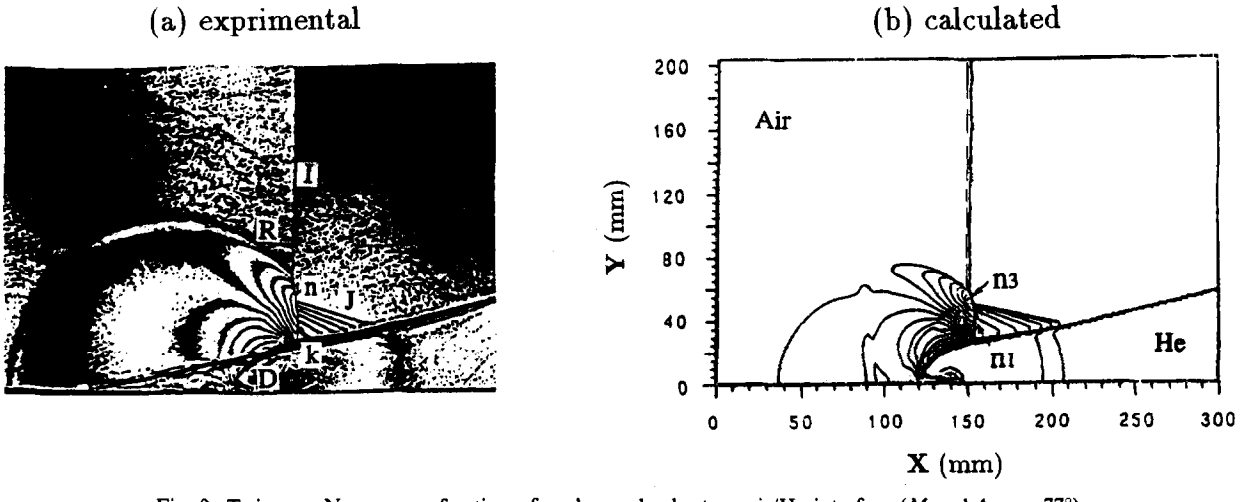

Fig. 9. Twin von Neumann refraction of a planar shock at an air/He interface ($M_s = 1.4$, $\alpha_i = 77°$).

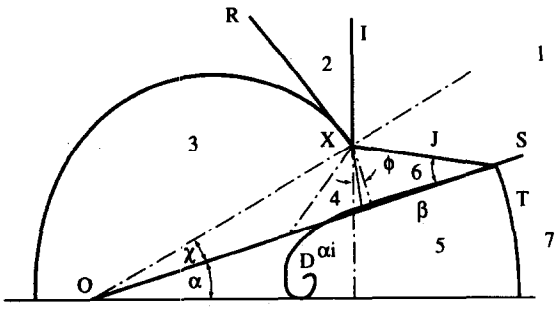

Fig. 10. Schematic illustration of the wave configuration of the free precursor von Neumann irregular refraction with critical angle α_{cf}.

limiting case when the Mach stem is perpendicular to the gaseous interface for irregular refraction at Slow/Fast interface. The limiting angle is equal to the angle of gas interface α. Thus, the angle corresponding to the Mach stem n_1 deflects from the incident shock and can be written as follows

$$\phi = \xi\alpha \quad 0 < \xi \leqslant 1. \tag{24}$$

Suggesting values of ξ range from 0.85 to 1; for the sake of simplicity, we assume ξ equal to 1.

According to the theory of shock reflection, the following relation is founded

$$M_s = M_1 \sin\gamma \tag{25}$$

with

$$\gamma = \alpha + \chi, \tag{26}$$

where χ denotes the angle between straight line OX and the initial gaseous interface OS (see Fig. 10). The deviation angle for the streamline crossing to the states from (1) via (2) to (3) is

$$\theta_n = \theta_r + \theta_i\,. \tag{27}$$

The deviation angle for the streamline crossing to the states from (1) via (6) to (4) is

$$\theta_m = \theta_k + \theta_j\,, \tag{28}$$

where θ is the deviation angle. The subscripts i, j, r and k indicate the incident shock I, the precursor shock, the reflected shock and the Mach stem, respectively. Since states (3) and (4) represent the same state, both deviation angles θ_n and θ_m must be equal to one another, that is

$$\theta_n = \theta_m\,. \tag{29}$$

Therefore, only one solution exists for critical angle α_{cf} according to eqn (29). To calculate the angle α_{cf}, we need to determine the strength of Mach stem M_{sn}. Based on the configuration of shock refraction as seen in Fig. 10, the following expression is given

$$u_{sn} = M_{sn}\cdot a_6 + u_{6n}\,, \tag{30}$$

where u_{sn} is the velocity of Mach stem, and a_6 denotes the speed of sound in the state (6), it can be obtained from

$$a_6 = \frac{\{[2k_1M_{sj}^2 - (k_1-1)][(k_1-1)M_{sj}^2 + 2]\}^{1/2}}{(k_1+1)M_{sj}}\,. \tag{31}$$

u_{6n} denotes a component of the velocity u_6 projecting to the direction of u_{sn}, and u_6 denotes the velocity of the flow in the state (6); u_6 and u_{sn} are given by

$$u_6 = \frac{2a_1}{k_1+1}\left(M_{sj} - \frac{1}{M_{sj}}\right) \tag{32}$$

$$u_{6n} = -u_6\cos(\gamma+\beta+\chi) \tag{33}$$

from (30) through (33), the strength of Mach stem M_{sn} can be written as follows

$$M_{sn} = \frac{1}{a_6}\left[M_s a_1 + \frac{2}{k_1+1}a_1\left(M_{sj} - \frac{1}{M_{sj}}\right)\times\cos(\gamma+\beta+\chi)\right]. \tag{34}$$

The pressure ratio for the state (4) and the state (6) P_4/P_6 is given by

$$\frac{P_4}{P_6} = \frac{2k_2M_{sn}^2 - (k_2-1)}{k_2+1}\,. \tag{35}$$

Thus, from eqns (34) and (35), the deviation angle for the streamline crossing to the Mach stem, θ_m, is obtained as

$$tg\theta_m = \frac{\dfrac{P_4}{P_6}-1}{1+k_2M_{sn1}^2-\dfrac{P_4}{P_6}}\left[\frac{\dfrac{2k_2M_{sn1}^2-(k_2-1)}{k_2+1}-\dfrac{P_4}{P_6}}{\dfrac{P_4}{P_6}+\dfrac{k_2-1}{k_2+1}}\right]^{1/2}, \tag{36}$$

where

$$M_{sn1} = \frac{M_{sn}}{\sin\gamma}\,. \tag{37}$$

The deviation angle θ_n for the streamline crossing to the states from (1) via (2) to (3) can be calculated by eqn (27). In this expression, both angles θ_i and θ_r need to be determined. The angle θ_i is the deviation angle for the streamline crossing to the states from (1) to (2). The following expression is obtained according to the shock wave relations.

$$tg\theta_i = -\frac{\dfrac{P_2}{P_1}-1}{1+k_1M_1^2-\dfrac{P_2}{P_1}}\left[\frac{\dfrac{2k_1M_1^2-(k_1-1)}{k_1+1}-\dfrac{P_2}{P_1}}{\dfrac{P_2}{P_1}+\dfrac{k_1-1}{k_1+1}}\right]^{1/2}, \tag{38}$$

where

$$\frac{P_2}{P_1} = \frac{2k_1M_1^2\sin\gamma - (k_1-1)}{k_1+1} \tag{39}$$

$$M_1 = \frac{M_s}{\sin\gamma}. \tag{40}$$

The deviation angle, θ_r, is given by

$$tg\theta_r = -\frac{\frac{P_3}{P_2}-1}{1+k_1M_2^2-\frac{P_3}{P_2}}\left[\frac{\frac{2k_1M_2^2-(k_1-1)}{k+1}-\frac{P_3}{P_2}}{\frac{P_3}{P_2}+\frac{k_1-1}{k_1+1}}\right]^{1/2}, \tag{41}$$

where M_2 is the Mach number for state (2)

$$M_2 = \left\{\frac{(k_1-1)M_s^2+2}{\sin^2(\gamma-|\theta_i|)[2k_1M_s^2-(k_1-1)]}\right\}^{1/2}. \tag{42}$$

Note that the pressures in states (3) and (4) are equal to one another. The pressure ratio for states (3) and (2), P_3/P_2, is written as follows:

$$\frac{P_3}{P_2} = \frac{P_4}{P_6}\frac{P_6}{P_1}\Big/\frac{P_2}{P_1}. \tag{43}$$

According to the triangular relations of the shock refraction structure shown in Fig. 10, the angle χ, is given by

$$\chi = \sin^{-1}\left(\frac{v_1\sin\gamma}{M_sa_1}\sin\beta\right)-\beta. \tag{44}$$

Using the analytical criteria above, we plot α_c as a function of M_s for three physical interfaces: air/He, CH_4/H_2, and CO_2/H_2 in Fig. 11. The properties for these gases are shown in Table 1. Figure 12 is the comparison of the critical angles between the results calculated by both the analysis method above and the numerical simulation.

6. CONSIDERATION FOR NUMERICAL SIMULATION RESULTS

Using the method described in section 2 and an upwind TVD scheme, a two-dimensional second-order accurate finite-difference code has been developed. Representative computational results are presented in Figs 3, 4(b), 8(b) and 9(b). To analyse the features of irregular shock refraction at gas interfaces, the case of TNR shown in Fig. 8(b) is used as the example for our discussion.

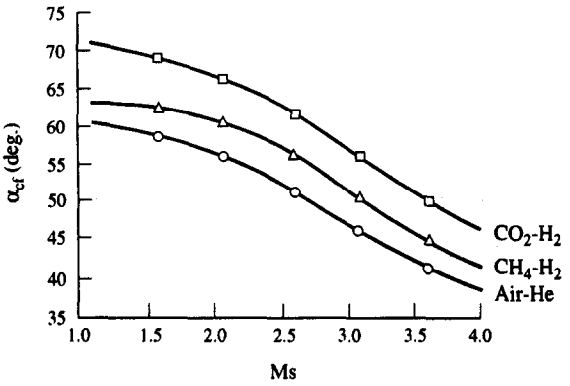

Fig. 11. Critical angle, α_{cf}, as a function of M_s for the transition from FNR into TNR.

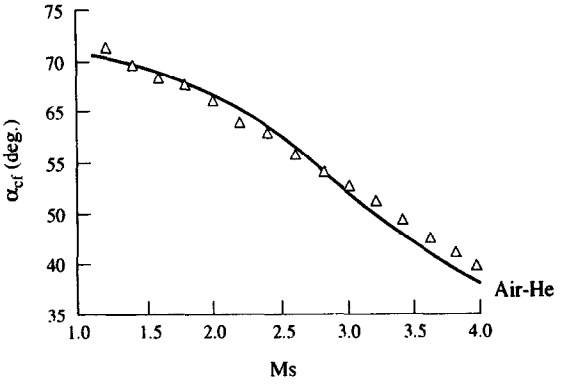

Fig. 12. Comparison of critical angles between the results of the analysis method and the numerical simulation from transition from FNR into TNR.

Figure 13 depicts the pressure distributions at different distances from the bottom surface corresponding to the case shown in Fig. 8. Figure 13 shows that a pressure spike occurs just behind the incident shock in state (4) (see Fig. 10) at a distance of 40 mm from the bottom surface. The maximum value of the pressure here is about 0.25 MPa. This pressure spike results from the interaction between the incident shock and the precursor wave. Thus, a high compression region is generated near the incident shock in state (4). The distribution of the velocity component in the x-direction, u, for this case is shown in Fig. 14. This figure shows that there is a velocity drop which appears just behind the incident shock in state (4) at a distance 20 mm from the bottom surface. It also suggests that a compression state occurs in this region. From Fig. 14 we can also see that the flow velocity u changes violently near the gaseous interface. Obviously, the minimum value of

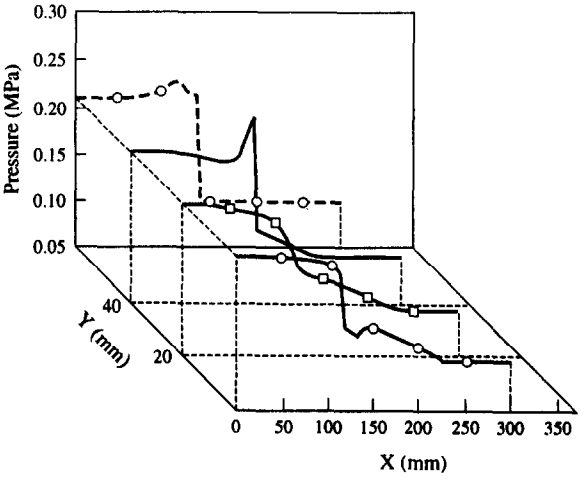

Fig. 13. Pressure distributions, air/He (M_s = 1.4, α_i = 77°).

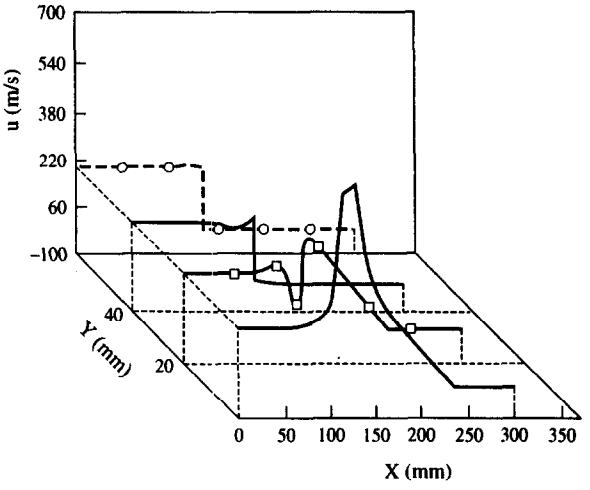

Fig. 14. Distributions of velocity component in the x-direction, air/He ($M_s = 1.4$, $\alpha_i = 77°$).

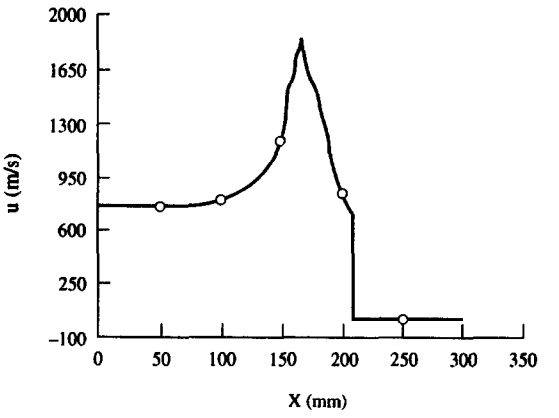

Fig. 16. Distribution of velocity component in the x-direction at the bottom surface, air/He ($M_s = 3.0$, $\alpha_i = 77°$).

the velocity in this region corresponds to the moving velocity of the gaseous interface. This velocity is less than the piston velocity u_2. In addition, both velocities of the flow in states (4) and (6) are not the same; rather, the difference is increased with enlargement of the strength of the incident shock.

Due to the velocity perturbation, the flow behind the system of refraction shocks produces a crater in the gases near the bottom surface, generating a precursor compression flow. This phenomenon can be seen in Fig. 8. The numerical simulation results show that this is a very complicated region of the flow field. As the flow distribution shows in Figs 13 and 14, the pressure is dropped and the flow is accelerated at the muzzle of the crater. The local velocity u reaches a very high value in this region. Interaction of the shock wave with density inhomogeneities reduces to the circulation deposition at the interface. A vortex ring will be formed in the perturbed interface.

Another evolution of a pertubated interface is shown in Fig. 15. In this case, the Mach number and the angle of the incident shock are 3.0 and 77°, respectively. Figure 16 depicts the distribution of the velocity component in the x-direction at the bottom surface of this case. The numerical results show that there is a pressure spike in front of the crater muzzle, and both pressure and the velocity of the flow reduce gradually at the bottom of the crater. Such distribution of the flow is similar to a jet flow. Due to the effects of impedances of the gas interface and shock reflection on the bottom surface, the front of the crater is curved upward and a vortex is formed over the crater front. A mixing between the two gases occurs by the vortex.

The crater shape depends upon the strength and the angle of the incident shock which are the main effects for the circulation deposition. The angle of the incident shock and the crater shapes remain similar even as the incident shock becomes stronger. The phenomenon can be seen in Figs 9 and 15. The numerical simulations and the experiments also show

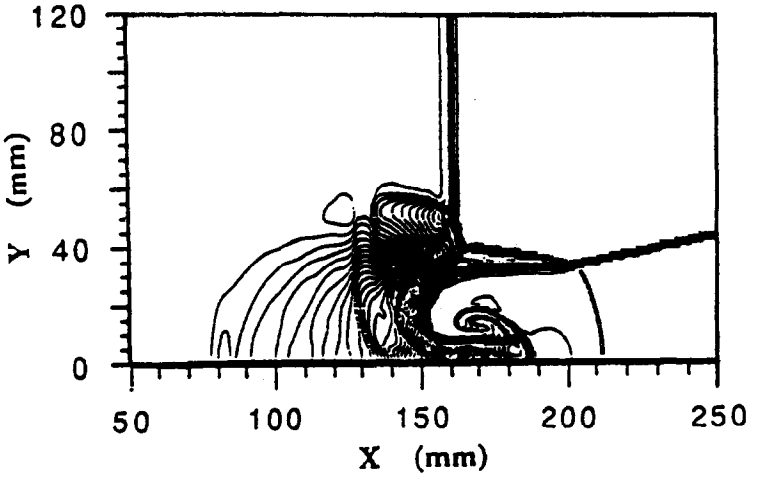

Fig. 15. Crater of the perturbated interface ($M_s = 3.0$, $\alpha_i = 77°$).

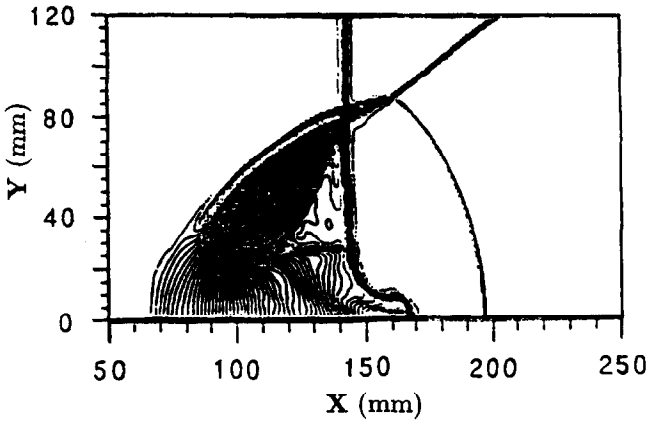

Fig. 17. Crater shape of gas interface for larger Mach number and angle of incident shock ($M_s = 3.5$, $\alpha_i = 52°$).

that the vortex only occurs in cases of larger angles of the incident shock. When the latter is small enough, the front surface of the crater becomes regular. Figure 17 gives an example for this case.

7. CONCLUDING REMARKS

We have demonstrated the numerical simulation of shocked-oblique S/F gaseous interface based on a Harten–Yee type second order accurate scheme. The refraction and the reflection of a planar shock wave at a gaseous interface were studied theoretically and experimentally. The results presented in this paper suggest the following conclusions:

(1) The double exposure holographic interferometry was used for a quantitative flow visualization of shock refraction at gaseous interfaces. The structures of the shock refraction, the deformations of the gaseous interface, and the phenomena of vortex in the flow can be obtained by the experiments.

(2) From comparing numerical and experimental results, the proposed numerical method is found to be in reasonable agreement with experiments. The method is also sufficiently accurate to be applied to the analysis of shock refraction at a gaseous interface.

(3) An analysis method for the conditions of shock structure transitions from BPR into FPR and FPR into TNR are presented. Agreement is obtained between the results which were calculated by both the analysis method and the numerical simulations. But a discrepancy appears for large Mach numbers of incident shock.

(4) The behaviour of the flow field in the region of the gaseous crater is similar to a high speed jet flow. A vortex, which mixes the two gases, is formed over the front of the crater resulting from the perturbed instability interface.

REFERENCES

1. J. Yang, T. Kubota and E. E. Zukoski, Applications of shock-induced mixing to supersonic combustion. *AIAA J.* **31**, 854–862 (1993).
2. D. L. Lindl, R. L. McCrory and E. M. Campbell, Progress toward ignition and burn propagation in inertial confinement fusion. *Phys. Today*, 32–40, September (1992).
3. L. Crum, Cavitation microjet as a contributory mechanism for Renal Calculi Disintegration in ESWL. *Urology J.* **140**, 1587–1590 (1988).
4. B. Sturtevant, The physics of shock focusing in the context of extra-corporeal shock wave lithotripsyi. *Proc. Int. Workshop on Shock Wave Focusing*, K. Takayama (Ed.), pp. 39–64. Shock Wave Research Center, Inst. of Fluid Sci. Tohoku Univ., Sendai, Japan (1990).
5. R. D. Richtmyer, Taylor instability in shock acceleration of compressible fluids. *Commun. Pure Appl Maths* **XIII**, 297–319 (1960).
6. E. E. Meshkov, Instability of a shock wave accelerated interface between two gases. *Izv. Akad. Nauk. SSSR, Mekh. Zhidk. Gaza* **5**, 151. NASA Tech. Trans. TT-F-13074 (1970).
7. H. Polachek and R. J. Seeger, On shock wave phenomena; refraction of shock waves at a gaseous interface. *Phys. Rev.* **84**, 922–929 (1951).
8. R. G. Jahn, The refraction of a plane shock wave at a fast-slow gas interface. *J Fluid Mech.* **1**, 457–489 (1956).
9. L. F. Henderson, The refraction of a plane shock wave at a gas interface, *J Fluid Mech.* **26**, 607–637 (1966).
10. A. M. Abd-El-Fattah, L. F. Henderson and A. Lozzi, Precursor shock waves at a slow/fast gas interface. *J. Fluid Mech.* **76**, 157–176 (1976).
11. A. M. Abd-El-Fattah and L. F. Henderson, Shock wave at a fast-slow gas interface. *J Fluid Mech.* **86**, 15–32 (1978).
12. L. F. Henderson, P. Colella and E. G. Pucett, On the refraction of shock wave at slow-fast gas interface. *J. Fluid Mech.* **224**, 1–27 (1991).
13. R. Samtaney and N. J. Zabusky, Circulation deposition on shock-accelerated planar and curved density-stratified interfaces: models and scaling laws. *J. Fluid Mech.* **269**, 45–78 (1994).
14. A. Harten, High resolution scheme for hyperbolic conservation lows. *J. Comp. Phys.* **49**, 357–393 (1983).
15. H. C. Yee, Upwind and symmetric shock-capturing scheme. NASA TM-89464 (1987).
16. J. Falcovit and G. Alfandary, Numerical simulation of the head-on reflection of a regular reflection. *Int. J. Numer. Methods Fluids* **17**, 1055–1077 (1993).